Journal of Applied Electrochemistry (2006) 36:97–103
DOI 10.1007/s10800-005-9045-3

Effects of ball milling on the physical and electrochemical characteristics of nickel hydroxide powder

Q.S. SONG[1,3,*], C.H. CHIU[2] and S.L.I. CHAN[3]
[1]*Department of Applied Chemistry, School of Chemical Engineering and Technology, Tianjin University, Tianjin 300072, P.R. China*
[2]*Department of Materials Science and Engineering, National Taiwan University, Taipei 106, Taiwan*
[3]*School of Materials Science and Engineering, University of New South Wales, Sydney, NSW 2052, Australia*
*(*author for correspondence, fax: +86-22-27403389, e-mail: weisu@public.tpt.tj.cn)*

Received 17 March 2005; accepted in revised form 15 July 2005

Key words: ball milling, electrochemical performance, nickel hydroxide, particle and crystallite size, pasted nickel electrode, structural characteristics

Abstract

Nickel hydroxide powder was modified by the method of ball milling, and the physical properties of both the ball-milled and un-milled nickel hydroxide were characterized by scanning electron microscopy, specific surface area, particle size distribution and X-ray diffraction. It was found that the ball milling processing could obviously increase the surface area, decrease the particle and crystallite size, and reduce the crystallinity of β-$Ni(OH)_2$, which was advantageous to the improvement of the electrochemical activity of nickel hydroxide powder. Electrochemical performances of pasted nickel electrodes using the ball-milled nickel hydroxide as an active material were investigated, and were compared with those of the electrodes prepared with the un-milled nickel hydroxide. Charge/discharge tests showed that the ball-milled nickel hydroxide electrodes exhibited better performances in the charging efficiency, specific discharge capacity, active material utilization and discharge voltage. The improvement of the performances of β-$Ni(OH)_2$ through ball milling could be attributed to the better reaction reversibility, higher coulombic efficiency, higher oxygen evolution potential and lower electrochemical impedance, as indicated by the cyclic voltammetry and electrochemical impedance spectroscopy studies. Thus, ball milling was an effective method to modify the physical properties and enhance the electrochemical performances of nickel hydroxide powder for the active material of rechargeable alkaline nickel batteries.

1. Introduction

Nickel hydroxide is the positive electrode material of rechargeable alkaline batteries (e.g. Ni/Cd, Ni/Fe, Ni/Zn, Ni/H_2 and Ni/MH). These nickel-based batteries are usually positive limited, so that the capacity and cycle life of the cells are determined mainly by the properties of nickel electrodes [1, 2]. In order to improve the cell performance, pasted nickel electrodes made from a porous nickel-foam substrate and an active material called spherical nickel hydroxide powder have been developed. With their high energy density and low cost relative to those of conventional sintered nickel electrodes, the pasted nickel electrodes have now been widely used in commercially available Ni/MH and Ni/Zn batteries [3–5]. The practical importance of nickel hydroxide materials and their electrochemical properties is not only limited to battery application, since nickel hydroxide or nickel oxide electrodes also find important applications in fuel cells, electrochemical capacitors, electrolysers, electrosynthetic cells and electrochromic devices.

As the discharged-state active material of the nickel electrodes, the physical and electrochemical characteristics of nickel hydroxide are the key to determine the property of the electrodes. Spherical nickel hydroxide powder with a particle size distribution from several microns to tens of microns has a high filling density and superior flow characteristics, which can provide an optimized pasting and a nickel-foam penetration process [6]. These physical properties of spherical nickel hydroxide are beneficial to the increase in the amount of the active material loaded in the electrode substrate and the improvement of energy density of the nickel electrodes. However, the electrochemical properties of spherical nickel hydroxide are inferior, e.g. the charging efficiency, active material utilization, electronic conductivity and proton diffusion ability are quite low [7]. So considerable

interest has centred on the improvement of the electrochemical activity of nickel hydroxide. Besides the composition (doping with cobalt, zinc, etc.) and the impurity level, some physical properties strongly influence the electrochemical performance of nickel hydroxide powder materials, such as the morphology, structural defects, surface area, degree of porosity, crystal form and crystallite size [8–10]. In particular, the crystallite size and crystallinity have been proven to be in strong correlation to the electrochemical activity of nickel hydroxide active materials. Studies [4, 11–13] have shown that nickel hydroxide with fine crystallite size and reduced crystallinity possesses a high chemical proton diffusion coefficient and an increased nickel utilization, giving excellent charge/discharge cycling behaviour.

Mechanochemical processing of materials by ball milling is an attractive new technique for preparing novel materials, e.g. amorphous and nanocrystalline materials. In comparison with other methods for the processing of materials, the ball milling technique is advantageous because it is based on simple processes, shows high efficiency, low energy consumption and cost. This technique has been widely applied to prepare hydrogen storage alloys for Ni/MH batteries and the electrode materials for lithium ion batteries [14–17]. It has been pointed out that the process of ball milling can decrease the particle and crystallite size of materials, and induce the continuous formation of structural defects through the cycling deformation of crystallites. In this work, the method of ball milling was used to modify the structural and electrochemical characteristics of the commercial spherical nickel hydroxide powder. The physical and electrochemical properties of the ball-milled nickel hydroxide were characterized and compared with those of the un-milled nickel hydroxide. The effect mechanism of ball milling and the relationship between the structural characteristics and electrochemical activity of nickel hydroxide were also examined. We report that ball milling is an effective method to modify the physical properties and enhance the electrochemical performances of nickel hydroxide powder for the active material of rechargeable alkaline nickel batteries.

2. Experimental details

2.1. *Ball milling processing and physical characterization of nickel hydroxide powders*

Commercial spherical $Ni(OH)_2$ powder (from NEXcell Battery Co., Ltd., containing co-precipitated 1.9 wt.% Co and 2.5 wt.% Zn) was milled in a ball mill. The ball to powder mass ratio was 8:1, and the duration of milling was scheduled between 24 to 120 h. The crystallographic structure of $Ni(OH)_2$ powders was characterized by X-ray diffraction (XRD) with a Rigaku diffractometer using Cu$K\alpha$ radiation ($\lambda = 1.542$ Å). Scanning electron microscopy (SEM) observation was performed using a LEO 1530 microscope. The specific surface area was evaluated by the Brunauer–Emmett–Teller (BET) nitrogen adsorption method using a CHEMBET-3000 surface area analyser. The particle size distribution of the powders was obtained using a Mastersizer 2000 particle size analyser. The properties of both the ball-milled and un-milled $Ni(OH)_2$ powders were examined and compared.

2.2. *Electrochemical characterization of nickel hydroxide powders*

Pasted nickel electrodes were prepared as follows: $Ni(OH)_2$ powder (before or after ball milling for 120 h), nickel powder (Inco T255) and CoO powder (Aldrich, −325 mesh) were mixed thoroughly in an agate mortar. A suitable amount of suspension containing 60 wt.% polytetrafluoroethylene (PTFE) (Aldrich) and 1.5 wt.% carboxymethyl cellulose (CMC) (Aldrich) was added to the mixed powder as a binder. The mixture was then blended to obtain a paste. The resulting paste was incorporated into a 2 cm × 2 cm nickel-foam substrate, to which a nickel ribbon was spot-welded as a current collector. Subsequently, the pasted electrodes were dried at 80 °C for 2–3 h and pressed at 175 MPa to assure good electrical contact between the substrate and the active material. The content of $Ni(OH)_2$ active material in the resultant electrodes was determined through the weight ratio of different electrode components.

Charge/discharge studies were conducted in a test cell, including the as-prepared nickel electrodes as the cathode and a hydrogen-storage alloy electrode as the anode. Polypropylene was used as the separator between the cathode and anode. The electrolyte solution consisted of 6 M KOH + 1 wt.% LiOH. The cell capacity was cathodically limited. The test cells were charged at a rate of 0.2 *C* for 6 h, and discharged at the same rate down to a cut-off voltage of 1.0 V. After several charge/discharge cycles for cell activation, the charge and discharge curves at the 0.5 *C* rate were obtained. The tests were performed on a Kikusui PF 40W-08 cycler.

For the cyclic voltammetry (CV) and electrochemical impedance spectroscopy (EIS) measurements, a three-compartment glass cell containing 6 M KOH + 1 wt.% LiOH electrolyte solution was used. The pasted nickel electrodes, which acted as the working electrode in the cell, were soaked in the electrolyte solution for 10 h before test. A hydrogen-storage alloy electrode with a capacity well in excess of the nickel electrodes was used as the counter electrode. For the reference electrode, a Hg/HgO (6 M KOH) electrode was employed, and the potential of the working electrode was monitored through a Luggin capillary with respect to the reference electrode. The nickel electrodes were activated by charge/discharge cycling before the experiments, and were then cycled several times by CV to obtain a stable profile. The voltammograms were recorded at a sweep rate of 0.1 mV s^{-1}, with a sweep potential range of 0.1–0.7 V vs Hg/HgO. For the EIS studies, the impedance spectra were recorded at a 5 mV amplitude of

perturbation, with a sweep frequency range of 20 kHz–1 mHz. The tests were performed using an Autolab PGSTAT30 system. All the electrochemical measurements were carried out at ambient temperature.

3. Results and discussion

3.1. *SEM and BET analyses*

Scanning electron micrographs at a high magnification for $Ni(OH)_2$ powders before and after ball milling are shown in Figure 1(a) and (b), respectively. It can be seen that $Ni(OH)_2$ particles consist of many tiny crystals. Spherical $Ni(OH)_2$ before ball milling is made up of stacks of thin plate-like crystals, and the surface porosity of the powder is low due to the relatively close stacking of the crystals. After ball milling for 120 h, the surface of $Ni(OH)_2$ particles changes to a different crystal texture with granular crystals and a high porosity.

From the BET measurement, the specific surface areas of $Ni(OH)_2$ powders before and after ball milling are 10 and 21 $m^2\ g^{-1}$, respectively. This indicates that the ball milling processing not only alters the surface morphology and crystal form of $Ni(OH)_2$ powder, but also increases the surface area of the powder material.

For the active material of nickel electrodes, a high surface porosity is beneficial to the penetration of the electrolyte into the electrode. Meanwhile, high specific surface area provides a high density of active sites and promotes intimate interaction of the active material with the surrounding electrolyte [7, 8]. Therefore better utilization of the ball-milled $Ni(OH)_2$ material is facilitated by the high porosity and surface area.

3.2. *Particle size distribution*

In order to investigate the effects of the ball-milling time on the particle size of $Ni(OH)_2$ powders, the particle size distribution of the powders was measured and the

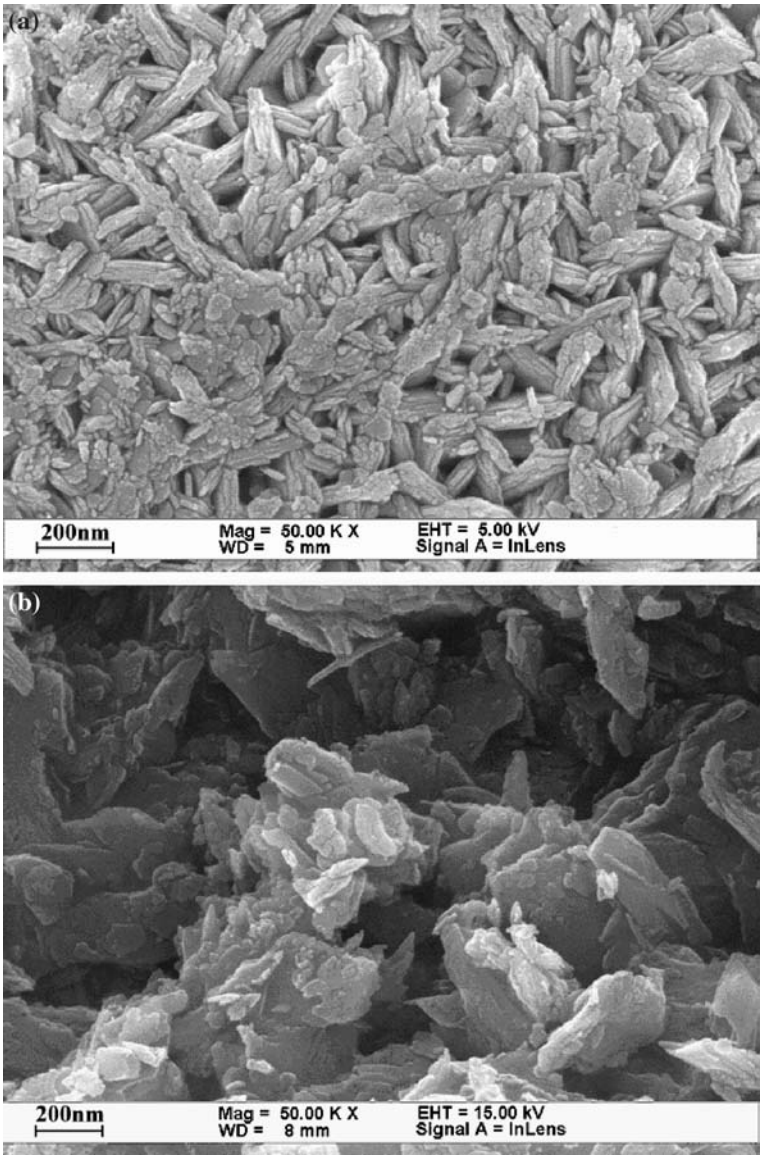

Fig. 1. SEM photographs for $Ni(OH)_2$ powders before (a) and after (b) ball milling.

average particle size (d_{50}) was obtained. Figure 2 shows the change of the average particle size of $Ni(OH)_2$ powders with the milling time. The particle size is markedly decreased during a 24 h of the milling time. When the milling time is beyond 24 h, the particle size is also decreased with the increase in the milling time, but the rate of the decrease in the particle size is lowered. The average particle size is decreased from 8.839 to 1.926 μm by ball milling when the milling time is reached at 120 h. This confirms that ball milling is an effective process making large particles become small ones.

3.3. *XRD patterns*

XRD patterns of $Ni(OH)_2$ powders before and after ball milling are presented in Figure 3(a) and (b), respectively. The characteristic diffraction peaks at (001)($d_{4.60}$), (100)($d_{2.70}$), (101)($d_{2.34}$), (102)($d_{1.76}$), (110)($d_{1.56}$) and (111)($d_{1.48}$) show that both these $Ni(OH)_2$ samples have a β-type crystal structure. β-$Ni(OH)_2$ crystallizes with a hexagonal brucite structure. The inter-sheet distance c of the layered structure of nickel hydroxide is represented by the d_{001} value. The d_{100} or d_{110} value corresponds to the Ni–Ni distance a in the layers of nickel hydroxide, where $a=[2/\sqrt{3}]d_{100}$ or $2d_{110}$ [18, 19]. The crystal parameters obtained from XRD patterns are listed in Table 1. It can been seen that the ball milling processing does not alter the basic crystal structure of β-$Ni(OH)_2$. However, compared with $Ni(OH)_2$ before ball milling, the ball-milled $Ni(OH)_2$ shows some different microstructural characteristics as revealed in the XRD patterns. The peaks corresponding to the (001), (101), (102) and (111) reflections in the XRD pattern of the ball-milled $Ni(OH)_2$ are noticeably broadened as compared to those in the pattern of the un-milled $Ni(OH)_2$. That is, a larger full-width of half-maximum intensity (FWHM) of these peaks is obtained with the ball-milled $Ni(OH)_2$.

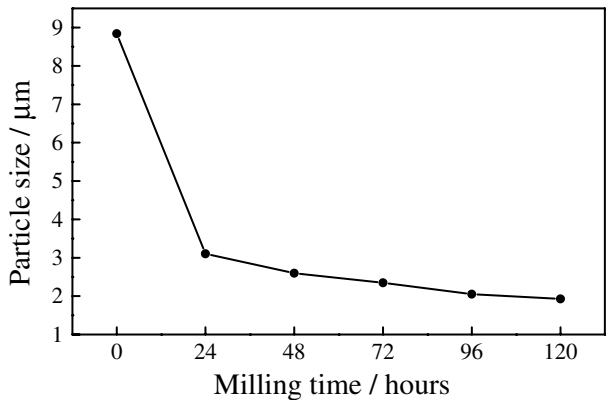

Fig. 2. The average particle size at the various milling time for $Ni(OH)_2$ powders.

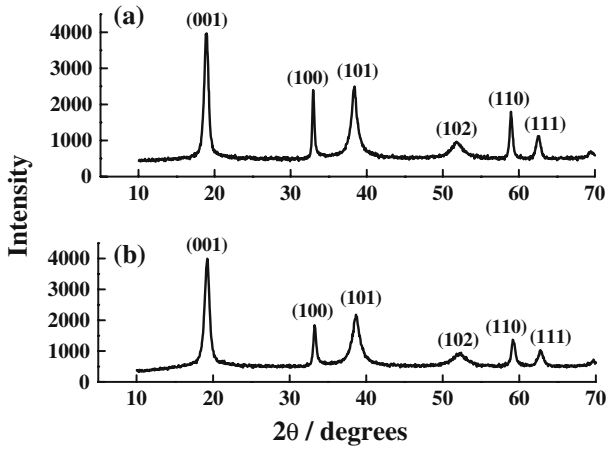

Fig. 3. XRD patterns for $Ni(OH)_2$ powders before (a) and after (b) ball milling.

The broadening of some of the diffraction lines [e.g. (001) and (hk0)] is directly related to the crystallite size [11, 20]. The crystallite size D, in the direction perpendicular to various diffraction planes can be estimated from the XRD lines using the Scherrer formula:

$$D = 0.9\lambda/B\cos(\theta) \quad (1)$$

where D is the crystallite size, λ represents the X-ray wavelength, B is the FWHM, and θ is the Bragg angle. The D values of $Ni(OH)_2$ calculated from (001) and (101) XRD peaks are given in Table 1. It indicates that the ball-milled $Ni(OH)_2$ has a smaller crystallite size as related to the un-milled $Ni(OH)_2$.

Furthermore, it has been pointed out that the abnormal broadening of the (10 l) reflection lines ($l \neq 0$) cannot be attributed only to the crystallite size. The existence of structural defects, such as stacking faults/growth faults and/or proton vacancies, also plays a very important role in explaining this broadening [11, 20, 21]. So, besides with a smaller crystallite size, the ball-milled $Ni(OH)_2$ should also possess more structural defects as compared to the un-milled $Ni(OH)_2$. Thus, ball milling is an effective method to decrease the crystallite size and increase the structural defects of nickel hydroxide powder.

It is widely accepted that the nickel electrode works as an insertion electrode for protons, the redox reaction of Ni(II)/Ni(III) in alkaline media can be expressed as:

$$NiOOH + H_2O + e^- \rightleftarrows Ni(OH)_2 + OH^- \quad (2)$$

which is believed to be a solid-state proton intercalation and de-intercalation reaction [22–25]. In the charge/

Table 1. Experimental results of XRD analysis for nickel hydroxide powders

Parameters	Un-milled $Ni(OH)_2$	Ball-milled $Ni(OH)_2$
Crystal type	β-$Ni(OH)_2$	β-$Ni(OH)_2$
Crystallite size calculated from (001) peak/nm	12.0	11.8
Crystallite size calculated from (101) peak/nm	8.0	7.8
Lattice parameter c/Å	4.60	4.60
Lattice parameter a/Å	3.12	3.12

discharge process, the proton insertion into and desertion from the hexagonal structure of nickel hydroxide occur reversibly, and the crystal structure of nickel hydroxide is maintained. The electrochemical activity of nickel hydroxide materials can be improved by increasing the chemical proton diffusion coefficient in $Ni(OH)_2$. The small crystallite size and low crystallinity (high density of structural defects) of nickel hydroxide powder are beneficial to the acceleration of the solid-state proton diffusion in $Ni(OH)_2$ lattice, and this will diminish the concentration polarization of protons during charge/discharge, leading to a better charge/discharge cycling behaviour. Thus, the ball-milled $Ni(OH)_2$ is envisaged to display a superior electrochemical behaviour as compared to the spherical $Ni(OH)_2$ before ball milling. This conclusion is corroborated by the following electrochemical studies.

3.4. *Charge/discharge tests for pasted nickel electrodes*

Figure 4 shows the typical charge and discharge curves at the 0.5 *C* rate for the pasted nickel electrode with the un-milled $Ni(OH)_2$ as the active material (code A) and the electrode prepared with the ball-milled $Ni(OH)_2$ (code B). The top-of-charge voltage of electrode B is lower than that of electrode A, which indicates that the former has a better chargeability and a lower intrinsic resistance. It is well known that the swelling of the nickel electrodes during cycling has detrimental effects on the performances of the nickel electrodes and batteries. Swelling reduces the integrity of the electrodes and causes a bad electrical contact between the active material and substrate. Consequently, the electrode performances are impaired by the decrease in the charging efficiency and cycle life of the electrodes [26, 27]. Swelling, as reflected by an increase in the thickness of the electrodes, is related to the formation of γ-NiOOH during cycling. During charging, the product β-NiOOH can be easily transformed into the less dense γ-NiOOH. This is especially true when the electrodes are subjected to overcharging or charging at a high rate [28]. Such a high charge current or charge voltage promotes the formation of γ-NiOOH. Thus, the formation of γ-NiOOH and the swelling of the nickel electrodes can be suppressed by the ball milling processing of $Ni(OH)_2$ because of the lowering of the charge voltage.

As shown in Figure 4, the depth-of-discharge (DOD) and specific discharge capacity of electrode B are larger than those of electrode A. Moreover, the discharge plateau of electrode B is also higher and more level than electrode A. This indicates that the ball milling processing not only can increase the discharge capacity and utilization of the nickel hydroxide active material, but can also improve the discharge voltage of the nickel electrodes. Given these findings, it can be concluded that the ball-milled $Ni(OH)_2$ experiences less polarization during the charge/discharge process. The modification effect of ball milling on $Ni(OH)_2$ is further studied by CV and EIS.

3.5. *CV measurements of pasted nickel electrodes*

The cyclic voltammograms of the pasted nickel electrodes A and B are shown in Figure 5. For both electrodes, one anodic nickel hydroxide oxidation peak, appearing at about 500 mV, is recorded prior to oxygen evolution. Similarly, one cathodic oxyhydroxide reduction peak at about 320–350 mV is observed on the reverse sweep. To compare the CV characteristics of the electrodes A and B, the results of the CV measurements are tabulated in Table 2.

The average of the cathodic and anodic peak potentials (E_{rev}) can be taken as an estimate of the reversible potential for the nickel electrodes, and the difference in the anodic and cathodic peak potentials ($\Delta E_{a,c}$) is a measure of the reversibility of the redox reaction. The ratio of the cathodic to anodic peak heights represents the coulombic efficiency of the electrode materials [8]. The experimental data in Table 2 show that the redox reactions are somewhat quasi-reversible for the pasted nickel electrodes A and B, as indicated by the relatively

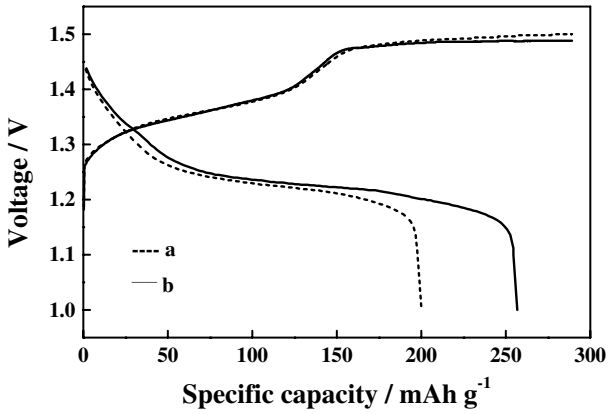

Fig. 4. Typical charge and discharge curves at the 0.5 *C* rate for pasted nickel electrodes prepared with $Ni(OH)_2$ powders before (a) and after (b) ball milling.

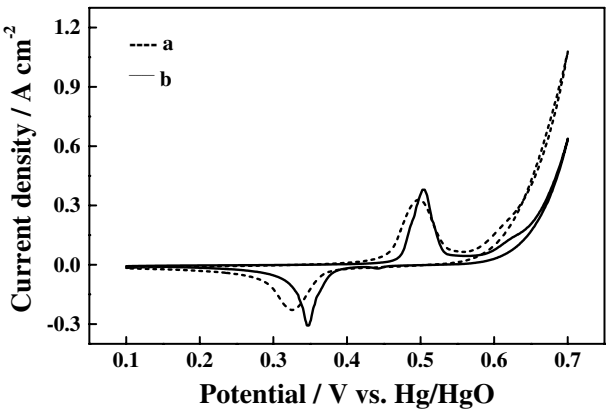

Fig. 5. Cyclic voltammograms for pasted nickel electrodes prepared with $Ni(OH)_2$ powders before (a) and after (b) ball milling.

Table 2. Experimental results of CV measurements for pasted nickel electrodes

Electrodes	Anodic peak potential E_a/mV	Cathodic peak potential E_c/mV	Average potential E_{rev}/mV	Peak separation $\Delta E_{a,c}$/mV	Oxygen evolution potential Eo_2/mV	Coulombic efficiency η/%
A	499	325	412	174	635	68
B	503	350	427	153	671	82

large $\Delta E_{a,c}$. However, the $\Delta E_{a,c}$ of electrode B is smaller than that of electrode A, which suggests that electrode B with the ball-milled $Ni(OH)_2$ has better reaction reversibility. Furthermore, electrode B also has a more anodic reversible potential and a higher coulombic efficiency compared to electrode A.

It is well known that oxygen evolution is the parasitic reaction during charging of nickel battery electrodes. Oxygen gas bubble formation may contribute significantly to electrode degradation by generating internal tensile stresses within the pores of the porous pasted nickel electrodes, which can ultimately affect the cycle life of the electrodes and batteries. Moreover, oxygen evolution reaction also lowers the charging and coulombic efficiency of the electrodes during the charge/discharge cycle [29, 30]. To investigate the effects of the ball milling processing of nickel hydroxide powder on the oxygen evolution reaction, the potentials at 300 mA cm^{-2} from the voltammograms are taken as an estimate of the potential for oxygen evolution. For this, the potentials on the return sweep required to produce 300 mA cm^{-2} of anodic current are adopted, since the return sweep can provide the best approximation of the steady-state condition with less interference from the nickel hydroxide redox reaction [31]. The results in Table 2 show that the oxygen evolution potential of electrode B shifts to a more positive value as related to electrode A, suggesting that oxygen evolution appears to be more difficult for electrode B than electrode A. Thus, a higher charging and coulombic efficiency can be obtained with electrode B due to the increase in the oxygen evolution potential. Furthermore, a higher oxygen evolution potential is also beneficial to lower the internal pressure and improve the cycle life of nickel-based rechargeable batteries.

As shown in Figure 5, both the anodic and cathodic peak current densities for electrode B are higher than those of electrode A at the same potential sweep rate. This indicates that more active materials can be utilized on the surface of electrode B during the charge/discharge process, suggesting that the nickel electrode with the ball-milled $Ni(OH)_2$ as the active material has a better electrochemical reactivity and a higher active material utilization. Thus, a higher charging efficiency and a greater discharge capacity can be obtained with electrode B.

Because the potential ranges for oxygen evolution and nickel hydroxide oxidation lie close to each other, the oxidizing current-density peak of the voltammograms may represent a combination of fluxes due to simultaneous oxidation and oxygen evolution reactions. This is particularly true for the porous pasted nickel electrodes in concentrated alkali solutions or at relatively high potential sweep rates [30]. Thus, the oxygen evolution reaction may have a strong effect on the anodic oxidation peak of the voltammograms. It can be seen from Figure 5 that the electrodes A and B have the almost same potentials for the anodic oxidation peaks. The reduction current-density peak is less influenced by the oxygen evolution reaction than the oxidation peak. The results in Table 2 show that the cathodic peak potential of electrode B is obviously shifted to a more anodic value as compared to that of electrode A. This observation is consistent with the above experimental results of the discharge voltage, implying again that electrode B has a higher discharge voltage and a smaller polarization during the charge/discharge process.

3.6. *EIS measurements of pasted nickel electrodes*

Figure 6 shows the electrochemical impedance spectra for the pasted nickel electrodes A and B. The impedance spectra of these two electrodes display a depressed semicircle resulting from the charge transfer resistance in the high-frequency region, and a slope related to the Warburg impedance appearing in the low-frequency region [32]. It can be seen that the impedance of electrode B with the ball-milled $Ni(OH)_2$ is smaller than that of electrode A with the un-milled $Ni(OH)_2$. This implies that the electrochemical reaction on electrode B proceeds more easily than that on electrode A.

In comparison with the spherical $Ni(OH)_2$ before ball milling, the ball-milled $Ni(OH)_2$ possesses a higher surface area, a smaller crystallite size and more structural defects. Therefore, the ball-milled $Ni(OH)_2$ powder

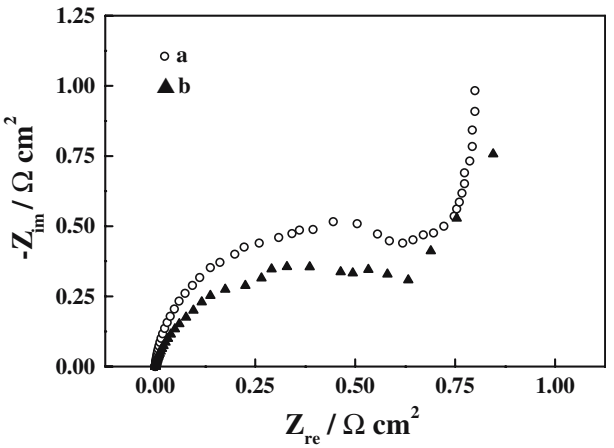

Fig. 6. Electrochemical impedance spectra of pasted nickel electrodes prepared with $Ni(OH)_2$ powders before (a) and after (b) ball milling.

provides an optimal degree of contact between the electrode and the electrolyte, and facilitates the intercalation/de-intercalation of protons or the rapid movement of both electrons and protons in the electrode. Accordingly, a smaller electrochemical reaction impedance and a better charge/discharge cycling behaviour can be obtained for the nickel electrode with the ball-milled $Ni(OH)_2$ as the active material.

4. Conclusions

The method of ball milling has been used to modify the physical and electrochemical characteristics of the commercial spherical nickel hydroxide powder. It is found that the ball milling processing not only can alter the surface morphology and crystal form of β-type nickel hydroxide powder, but can also increase the surface area of the powder material. The basic crystal structure of β-$Ni(OH)_2$ does not change after ball milling. However, compared with the un-milled β-$Ni(OH)_2$, the ball-milled β-$Ni(OH)_2$ possesses more structural defects and smaller sizes of particles and crystallites. These physical and structural characteristics are advantageous to the improvement of the electrochemical activity of nickel hydroxide powder.

Electrochemical measurements reveal that pasted nickel electrode using the ball-milled $Ni(OH)_2$ as the active material exhibits superior charge/discharge performances in comparison with those of the electrode prepared with the un-milled $Ni(OH)_2$. That is, a greater discharge capacity, better chargeability and a higher discharge voltage can be obtained with the ball-milled nickel hydroxide electrode. The improvement of the performances of nickel hydroxide powder through the ball milling processing can be attributed to the better reaction reversibility, higher coulombic efficiency, higher oxygen evolution potential and lower electrochemical impedance, as indicated by the cyclic voltammetry and electrochemical impedance spectroscopy studies. Thus, ball milling is an effective method to modify the physical properties and enhance the electrochemical performances of nickel hydroxide powder for the active material of rechargeable alkaline nickel batteries.

Acknowledgements

This work was supported by the Tianjin Municipal Natural Science Foundation of China (Grant No. 05YFJMJC09900), and by the Project-sponsored by SRF for ROCS, the Ministry of Education of China (Grant No. 2004-176).

References

1. A.K. Shukla, S. Venugopalan and B. Hariprakash, *J. Power Sources* **100** (2001) 125.
2. U. Köhler, C. Antonius and P. Bäuerlein, *J. Power Sources* **127** (2004) 45.
3. M. Oshitani, H. Yufu, K. Takashima, S. Tsuji and Y. Matsuma, *J. Electrochem. Soc.* **136** (1989) 1590.
4. K. Watanabe, T. Kikuoka and N. Kumagai, *J. Appl. Electrochem.* **25** (1995) 219.
5. W. Taucher-Mautner and K. Kordesch, *J. Power Sources* **132** (2004) 275.
6. I. Munehisa and A. Norikatsu, Eur. Patent No. EP 0523284 (1993).
7. Q.S. Song, Y.Y. Li and S.L.I. Chan, *J. Appl. Electrochem.* **35** (2005) 157.
8. P.V. Kamath and G.N. Subbanna, *J. Appl. Electrochem.* **22** (1992) 478.
9. G. Gille, S. Albrecht, J. Meese-Marktscheffel, A. Olbrich and F. Schrumpf, *Solid State Ionics* **148** (2002) 269.
10. Q.S. Song, Z.Y. Tang, H.T. Guo and S.L.I. Chan, *J. Power Sources* **112** (2002) 428.
11. M.C. Bernard, R. Cortes, M. Keddam, H. Takenouti, P. Bernard and S. Senyarich, *J. Power Sources* **63** (1991) 247.
12. C. Delmas and C. Tessier, *J. Mater. Chem.* **7** (1997) 1439.
13. R.S. Jayashree, P.V. Kamath and G.N. Subbanna, *J. Electrochem. Soc.* **147** (2000) 2029.
14. A.Kr. Singh, A.K. Singh and O.N. Srivastava, *Int. J. Hydrogen Energy* **18** (1993) 567.
15. C. Rongeat and L. Roué, *J. Power Sources* **132** (2004) 302.
16. M.N. Obrovac, O. Mao and J.R. Dahn, *Solid State Ionics* **112** (1998) 9.
17. L.J. Ning, Y.P. Wu, S.B. Fang, E. Rahm and R. Holze, *J. Power Sources* **133** (2004) 229.
18. P. Oliva, J. Leonardi, J.F. Laurent, C. Delmas, J.J. Braconnier, M. Figlarz, F. Fievet and A. Guibert, *J. Power Sources* **8** (1982) 229.
19. C. Faure, C. Delmas and M. Fouassier, *J. Power Sources* **35** (1991) 279.
20. C. Tessier, P.H. Haumesser, P. Bernard and C. Delmas, *J. Electrochem. Soc.* **146** (1999) 2059.
21. S. Deabate, F. Fourgeot and F. Henn, *J. Power Sources* **87** (2000) 125.
22. R. Barnard, C.F. Randell and F.L. Tye, *J. Appl. Electrochem.* **10** (1980) 109 and 127.
23. J.W. Weidner and P. Timmerman, *J. Electrochem. Soc.* **141** (1994) 346.
24. K. Watanabe and N. Kumagai, *J. Power Sources* **76** (1998) 167.
25. S. Motupally, C.C. Streinz and J.W. Weidner, *J. Electrochem. Soc.* **145** (1998) 29.
26. M. Oshitani, Y. Sasaki and K. Takashima, *J. Power Sources* **12** (1984) 219.
27. M. Oshitani, T. Takayama, K. Takashima and S. Tsuji, *J. Appl. Electrochem.* **16** (1986) 403.
28. D. Singh, *J. Electrochem. Soc.* **145** (1998) 116.
29. S.J. Lenhart, D.D. Macdonald and B.G. Pound, *J. Electrochem. Soc.* **135** (1988) 1063.
30. K.P. Ta and J. Newman, *J. Electrochem. Soc.* **146** (1999) 2769.
31. D.A. Corrigan and R.M. Bendert, *J. Electrochem. Soc.* **136** (1989) 723.
32. M.A. Reid and P.L. Loyselle, *J. Power Sources* **36** (1991) 285.